

## Abstract

The dense seismic AlpArray network provides ideal conditions for ambient-noise based studies. We use the available wealth of data to investigate the homogeneity of the noise field and look at the azimuthally anisotropic structure. Azimuthal anisotropy at shallow depths can be caused by stress-parallel microcracks (Kern et al. 1990) or due to shape-preferred orientation (faults, folds). Another source of anisotropy is the alignment of crystals such as olivine, amphibole or biotite, mostly in strain direction (Nicolas and Christensen, 1987; Barruol et al., 1993). Only few studies have looked at the anisotropic fabric of the crust (Fry et al., 2010; Lu, 2019; Schippkus et al., 2019) and it is still not well understood. We apply a new, simple method (Eikonal tomography, Lin et al., 2009) to determine anisotropic Rayleigh-wave phase-velocity maps for the entire Alpine orogen at a broad frequency range (3 - 80s). At very short periods, the anisotropic fast axis orientation aligns approximately parallel to the principal stress direction. Exceptions in the Po- and Molasse basin may be due to E-W oriented fault structures or spurious effects from very large velocity gradients. In mid-crustal levels, an arc parallel pattern of fast axis is observed which gradually turns into an arc-

perpendicular one at deeper crustal layers. This is observed in most of the Alpine crust, except in the eastern Alps which are influenced by an eastward extrusion (Frisch et al. 1998). This could indicate that the eastward movement is not confined to a single detachment fault but affects the entire crust at a broad depth range.

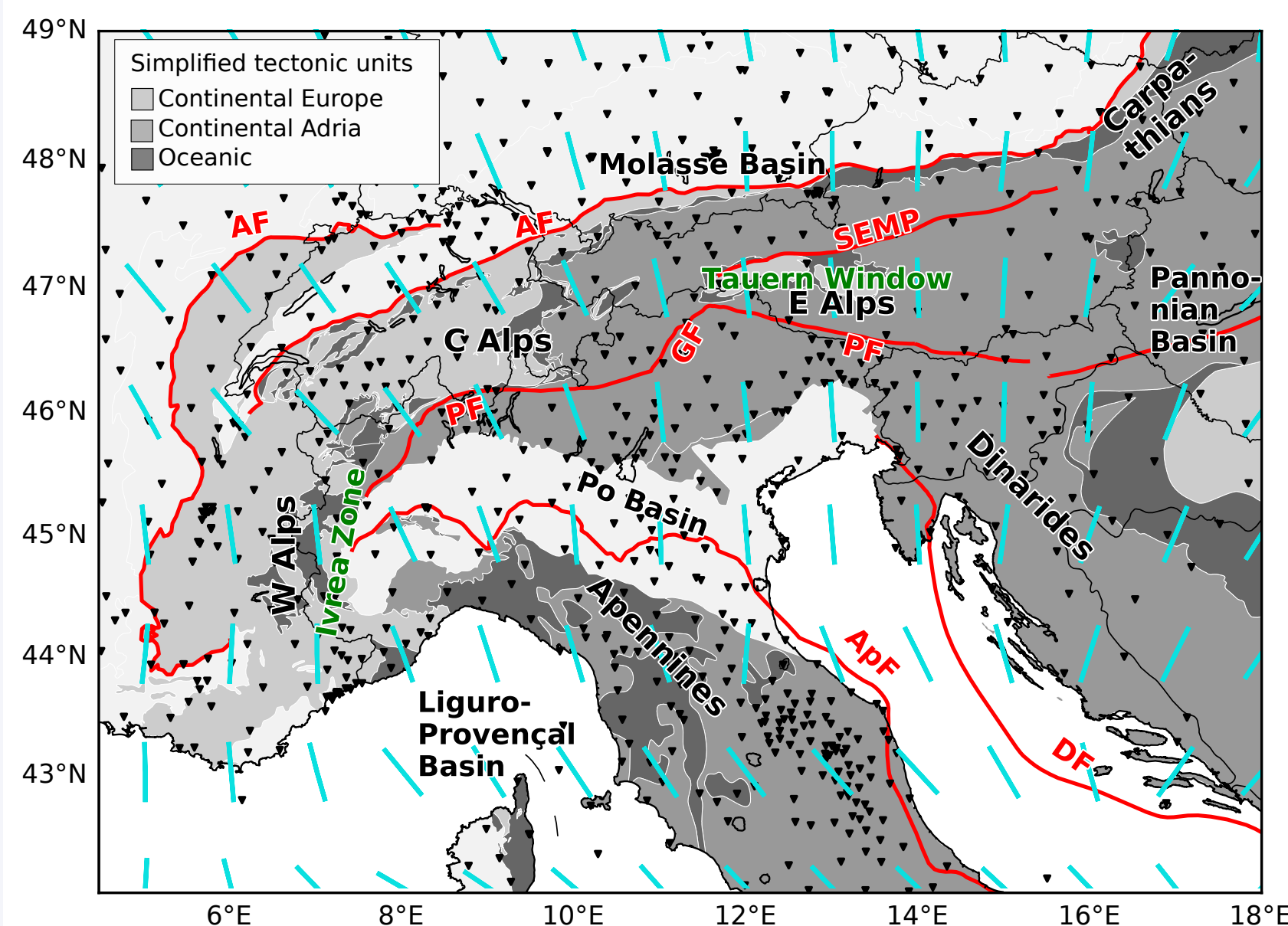


Figure 1: Tectonic overview map showing station locations (black triangles, temporary AlpArray and permanent) and simplified principal stress field (light blue, Heidbach et al., 2016). AF Adriatic Front, ApF Apenninic Front, DF Dinaric Front, PF Periadriatic Fault, GF Giudicarie Fault, SEMP Salzach-Ennstal-Mariazell-Puchberg fault. Tectonic units and major lineaments simplified from Handy et al. (2010).

## Anisotropy from Eikonal tomography

The Eikonal tomography method uses the gradient of the travel-time field to derive propagation velocities and directions (Lin et al., 2009). We use a smooth interpolation algorithm to get the travel-time field from all available central stations (Fig. 2). Stations close to large travel-time gradients are discarded and areas where too strong velocity deviations appear or where the closest station is too far away masked. A phase-velocity map is obtained for each available central station. The propagation direction and the velocities recorded for each grid cell are used to determine the anisotropic fast axis amplitude and direction. The anisotropic fast axis show the largest amplitudes at short periods. The results at intermediate periods are in good agreement with the previous work of Fry et al. (2010).

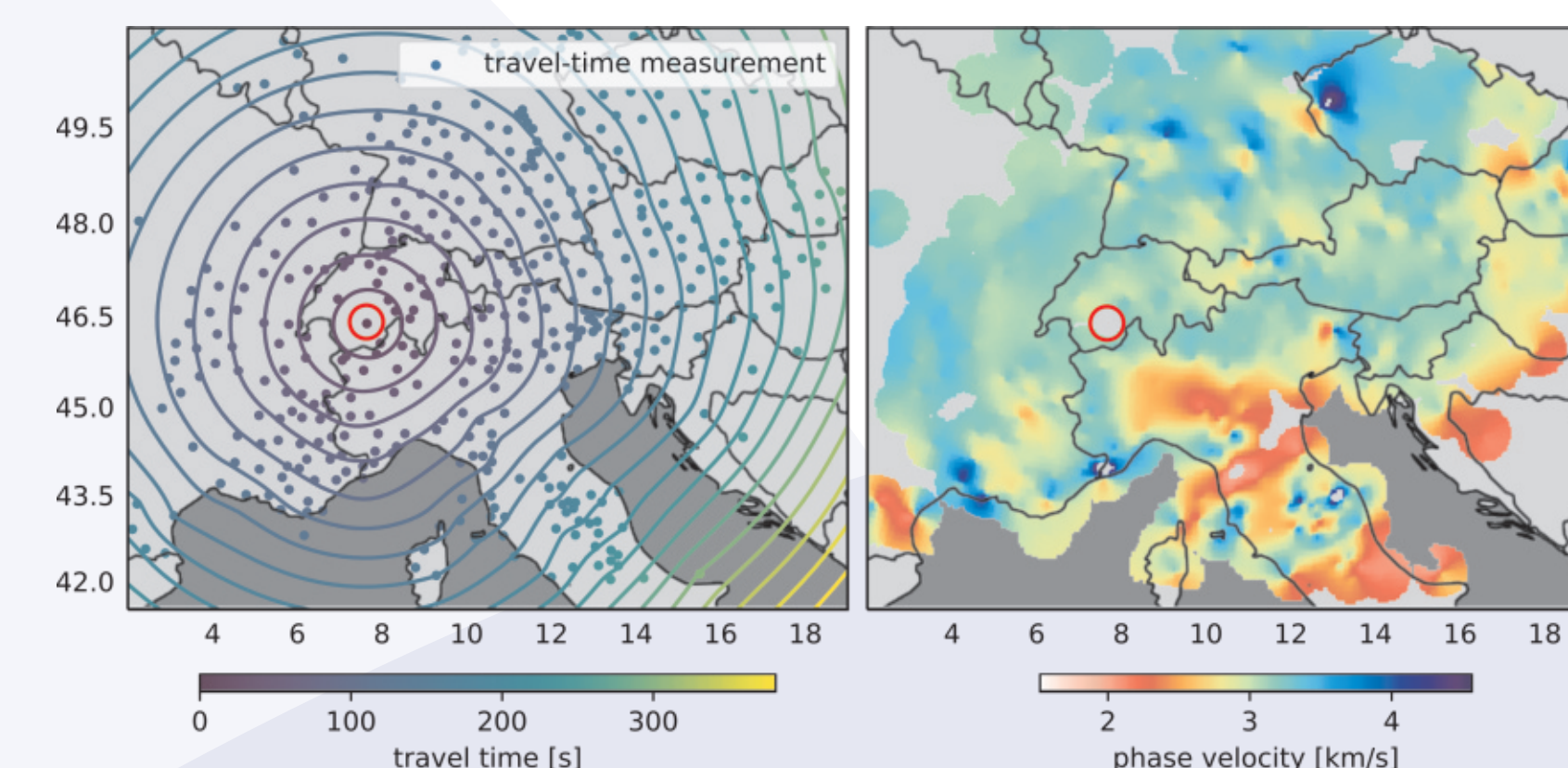
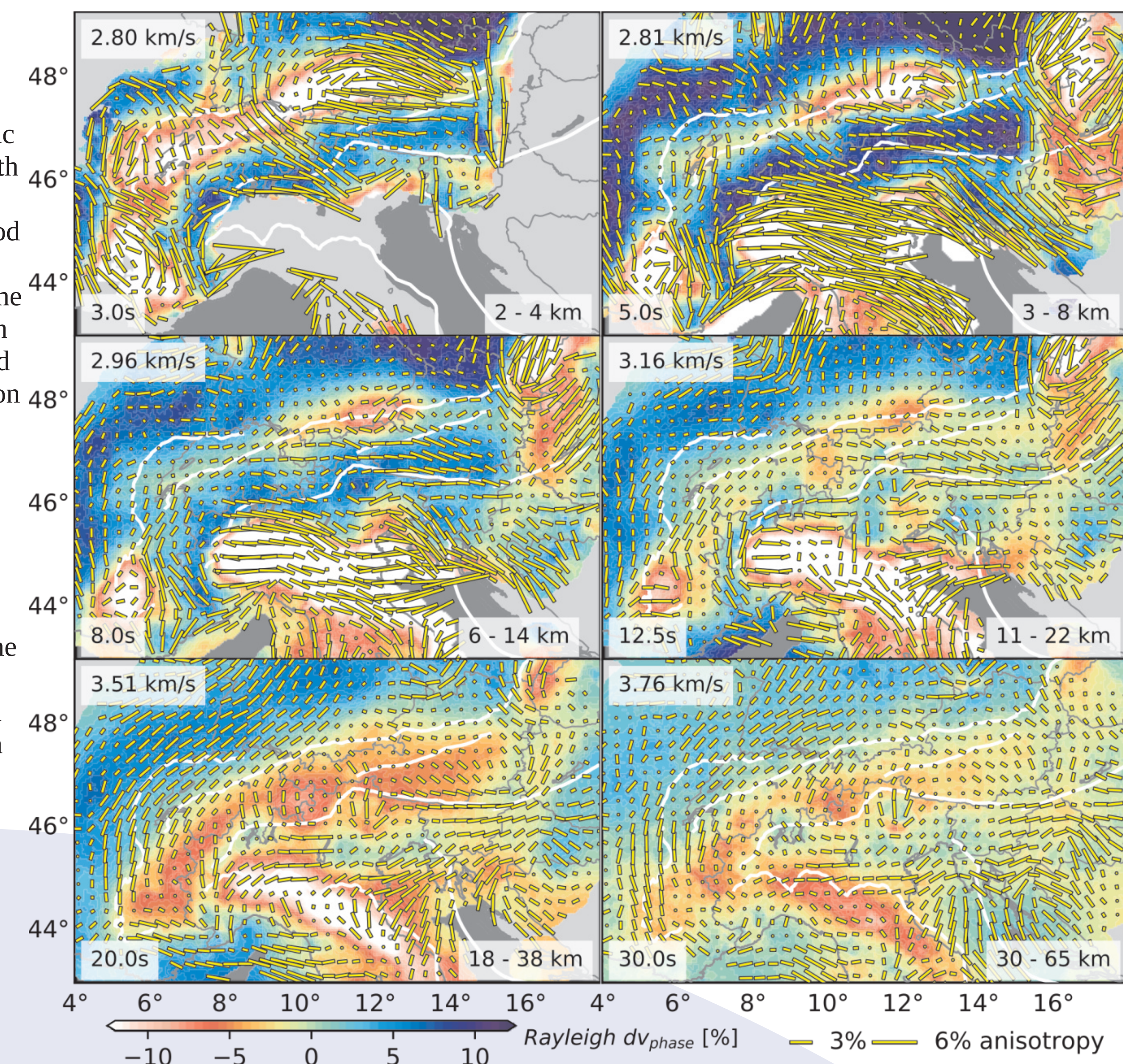


Figure 3 (right): Rayleigh phase velocity and anisotropic fast axis direction and strength at different periods. The isotropic velocities are in good agreement with previous works (Kästle et al. 2018). The anisotropic fast-axis direction at short periods can be related to the principal stress direction (Fig. 1) in many parts of the map.

Figure 2 (left): Example of the Eikonal tomography procedure for a single central station for data measured at a period of 10 s. The left panel shows phase travel-time measurements, interpolated travel-time field. The right panel shows the phase velocities. The final phase-velocity map is created by stacking the maps for all available central stations.



## Data processing

### Preprocessing steps

- + event removal (local and global,  $M > 2$ )
  - + removing high-energy windows
  - + filtering & downsampling
  - + instrument response removal
- procedure modified from L. Ermert (github.com/lermert/ants\_2)

### Crosscorrelation steps

- + cutting into 1hr windows
  - + transformation to frequency domain
  - + spectral whitening
  - + frequency domain cross-correlation
  - + stacking windows with 60% overlap
- (github.com/ekaestle/amb\_noise\_tools)

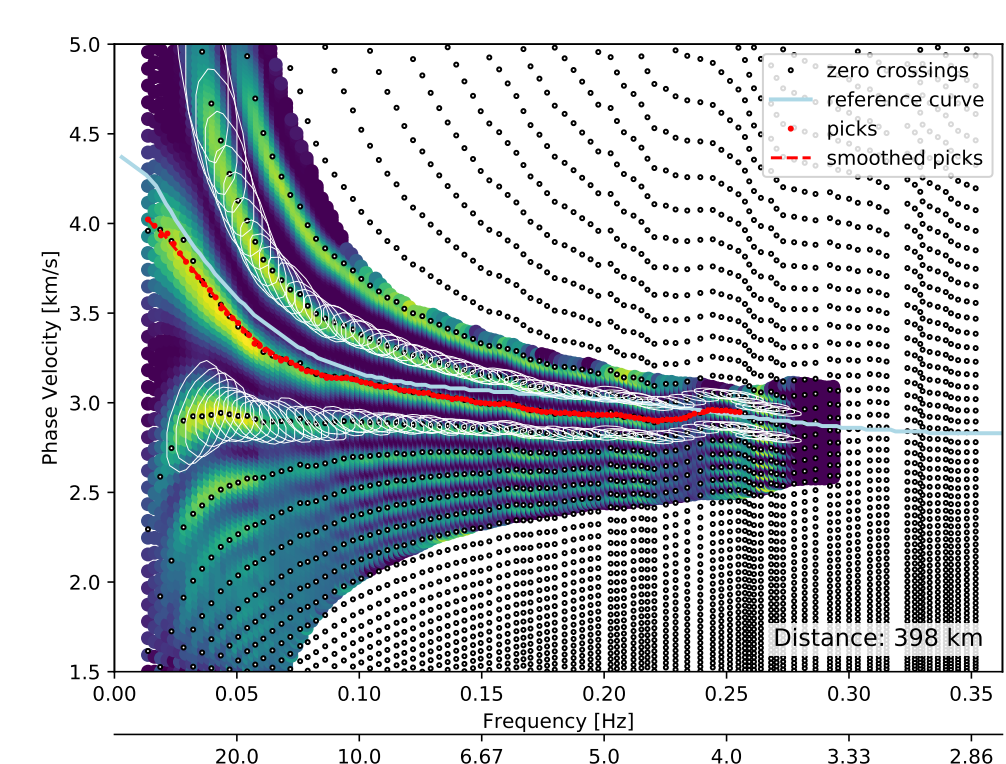


Figure 4: Picking phase-velocity curve from the smoothed zero-crossings of the Bessel function (stacked correlation in the frequency domain).

### Phase-velocity picking

- + velocity filtering
  - + zero-crossing smoothing
  - + only keeping measurements that give the same phase-velocity for the positive and negative time correlations (60% discarded)
- (github.com/ekaestle/amb\_noise\_tools)

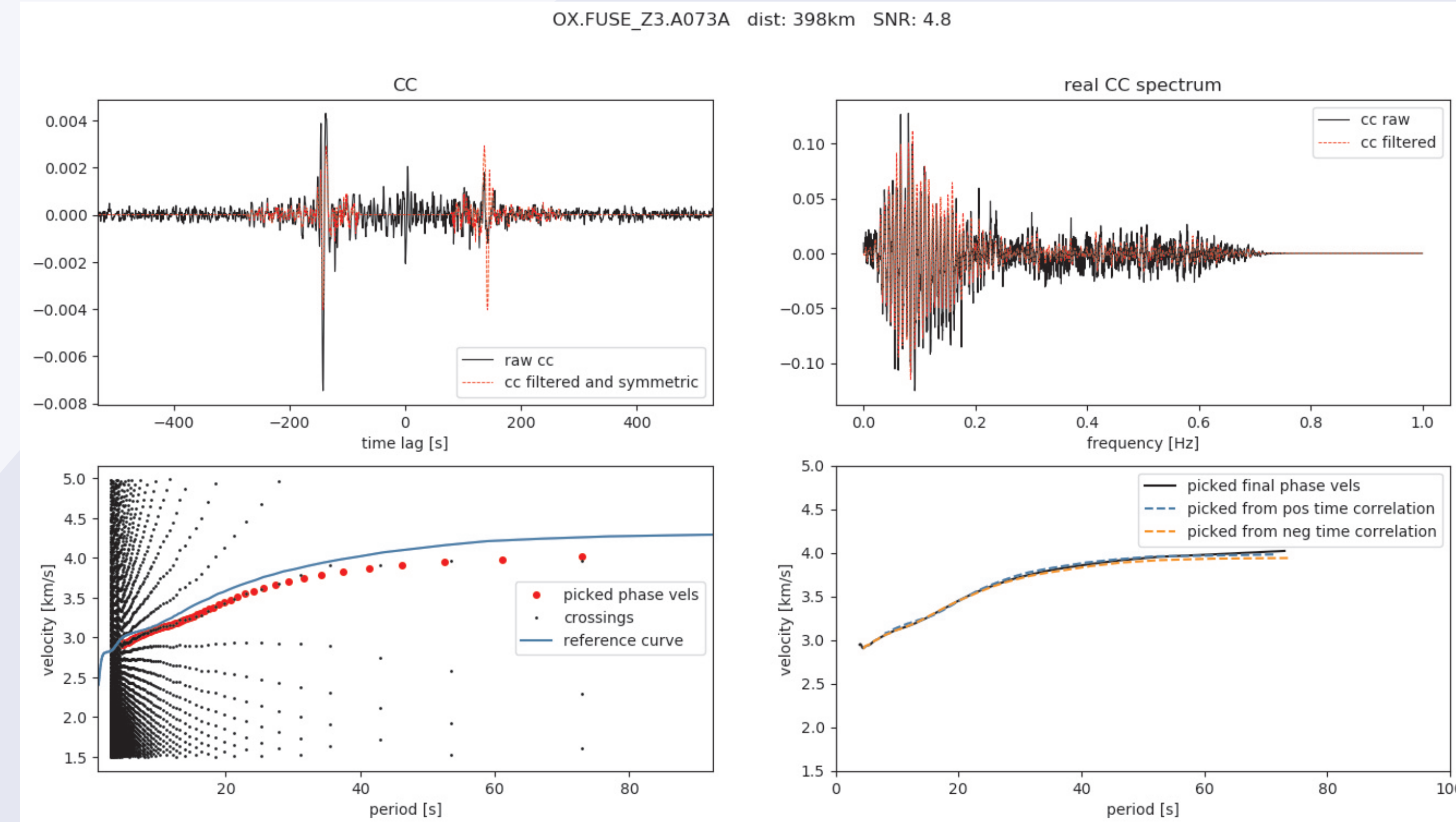


Figure 5: Stacked cross-correlation for one station pair in the time domain (top left) and in the frequency domain (top right). Dashed lines show the cross-correlations after velocity filtering. Bottom plots show the zero crossings of the cross-correlation spectrum and the picked phase-velocity curve.

## Noise sources

The ambient-noise method is based on the assumption of an equipartitioned wave-field (equal source energy from all directions) - a prerequisite that is never met. Studying the noise source distribution helps to understand the potential bias of this method and can be used to back-project to the source locations. Seasonal variations are due to the change of storm season in winter/summer in the two hemispheres.



Figure 6 (left): Variation of the signal-to-noise ratio (SNR) in the study region around the secondary microseismic peak (7s) as a proxy of the noise source direction. The SNR is normalized by the number of stacked days for each cross correlation. A longer red bar indicates a higher SNR and points towards the source region. A preferential ENE-WSW orientation can be observed. Plot only includes the summer months.

Figure 7 (right): Same as left figure but for the winter months.



## Anisotropy in the basins

The presented model is the first one to show the azimuthally anisotropic structure at a large frequency range. New results include the large E-W oriented amplitudes at 3-5s in the sedimentary basins. The cannot be explained with the direction of the principal stress axis (Fig. 1), but it could be caused by strong internal faulting as documented in active seismic sections (e.g., Pieri 1981; Bachmann et al., 1992).

Synthetic tests show that the Eikonal method is able to resolve structures with slightly smaller size than the average station spacing (Fig. 8) and reconstruct the anisotropy pattern in areas where a good data coverage is given. However, it is known that the method only works in smoothly varying

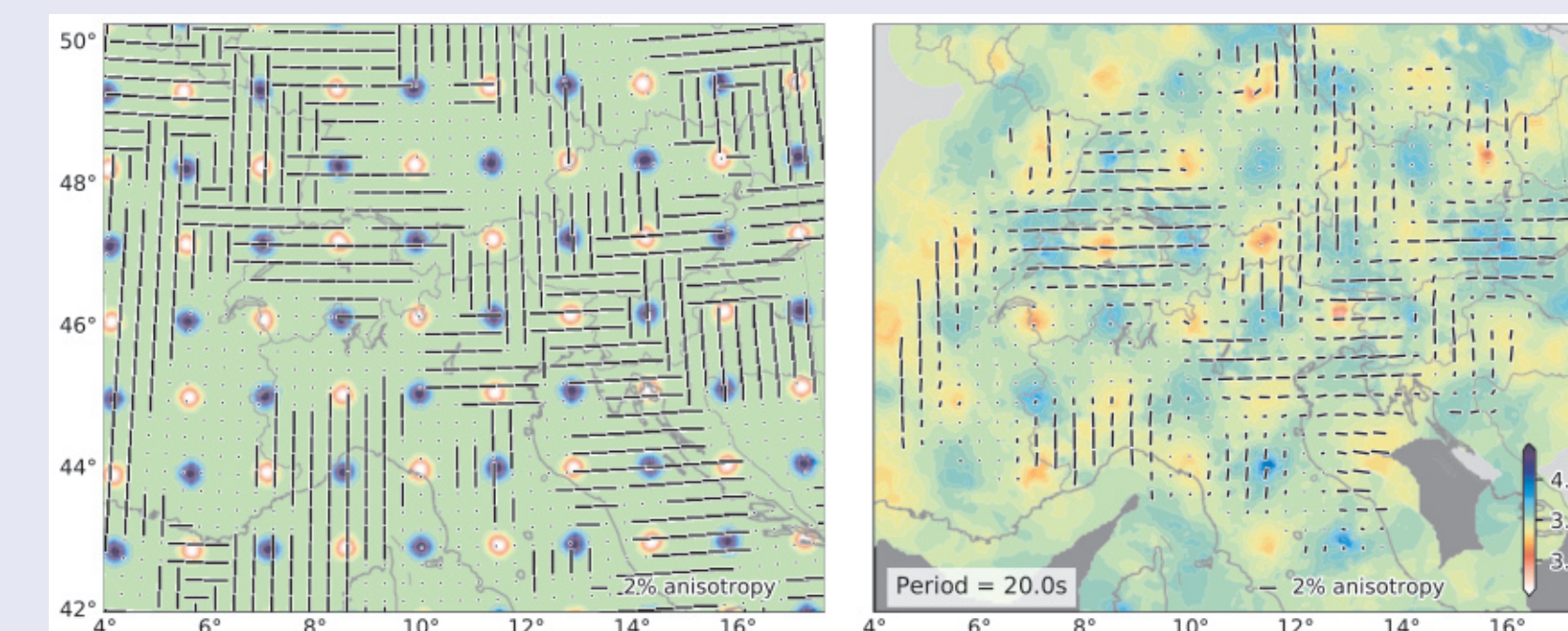


Figure 8: Synthetic test for an anisotropic medium with spikes of 30 km diameter and 10% velocity variation. The average station spacing is 50 km. The recovered isotropic model is smoothed, the anisotropy pattern is well reconstructed with some errors at the boundaries between domains of differently oriented fast-axis directions.

**Acknowledgements:** We thank the Obspy developers, ORFEUS for providing their data service, the respective AlpArray partner organizations for providing the data, Laura Ermert and Kees Weemstra for the automated processing scripts for ambient-noise data. The models were created with the help of the high-performance clusters of the ETH Zurich and FU Berlin.

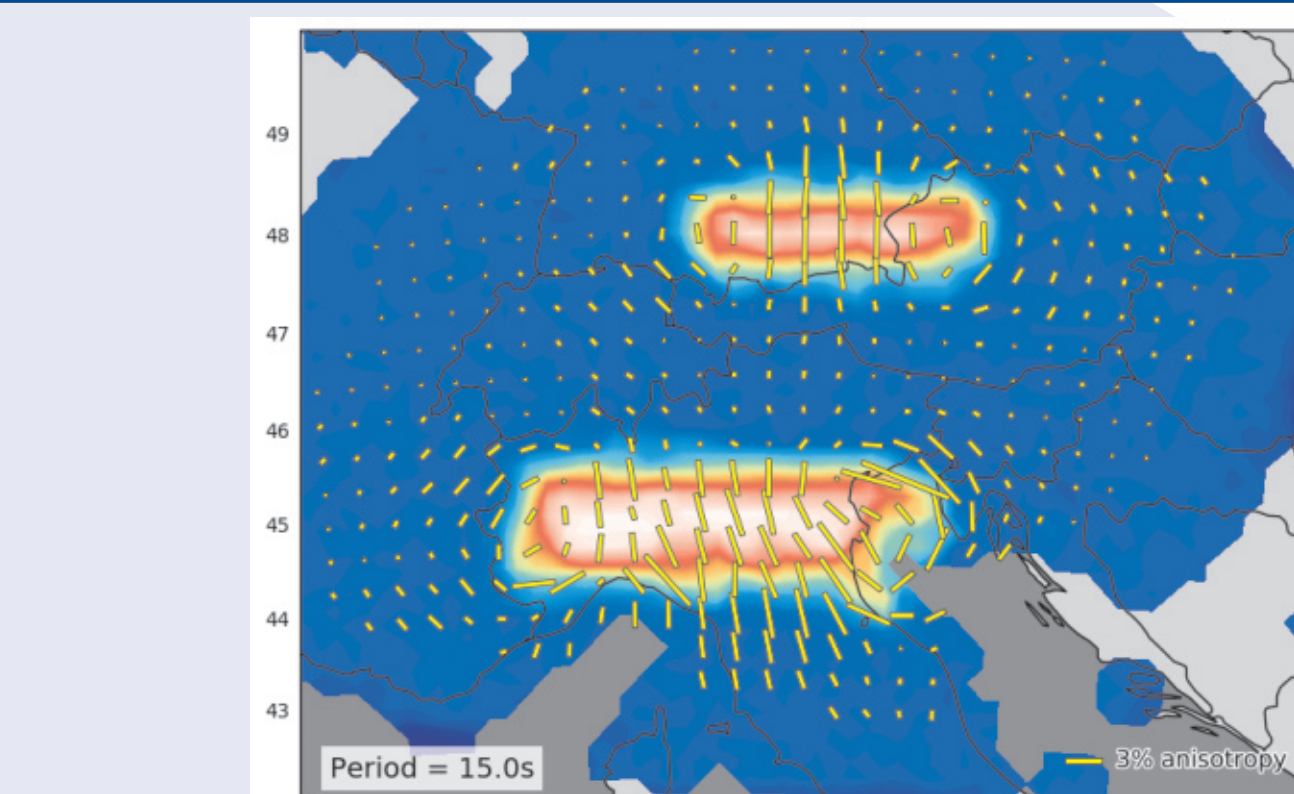


Figure 9: Recovered model from a purely isotropic synthetic input model with areas of 30% velocity deviation. The large velocity contrast causes the spurious anisotropy of around 1% (note the different scale compared to Fig. 8). media, strong velocity gradients introduce spurious velocity variations that increase the standard error and cause wrong anisotropic amplitudes (Fig. 9, Lin and Ritzwoller, 2011). This could also explain the strong anisotropy amplitudes in the sedimentary basins (Fig. 3). The expected bias would, however, only explain up to 2% of the observed anisotropy and is expected to be N-S oriented.

**References:** Bachmann, G. H., & Müller, M. (1992). Sedimentary and structural evolution of the German Molasse Basin. *Eclogae Geologicae Helveticae*, 85(3), 519-530.  
 Barruol, G., & Mairprêtre, D. (1993). 3-D seismic velocities calculated from lattice-preferred orientation and reflectivity of a lower crustal section: examples of the Val Sesia zone, northern Italy. *Geophysical Journal International*, 115(3), 1169-1188.  
 Frisch, W., Kuhlmann, J., Dunkl, L., & Brügel, A. (1998). Palaeogeographic reconstruction and topographic evolution of the Eastern Alps during late Tertiary tectonic extrusion. *Tectonophysics*, 297(1-4), 1-15.  
 Fry, B., Deschamps, F., Kissling, E., Stehly, L., & Giardini, D. (2010). Layered azimuthal anisotropy of Rayleigh wave phase velocities in the European Alpine lithosphere inferred from ambient noise. *Earth and Planetary Science Letters*, 297(1-2), 95-102.  
 Handy, M. R., Schmid, S. M., Bousquet, R., Kissling, E., & Bernoulli, D. (2010). Reconciling plate-tectonic reconstructions of Alpine Tethys with the geological-geophysical record of spreading and subduction in the Alps. *Earth-Science Reviews*, 102(3-4), 121-158.  
 Lin, F. C., Ritzwoller, M. H., & Snieder, R. (2009). Eikonal tomography: surface wave tomography by phase front tracking across a regional broad-band seismic array. *Geophysical Journal International*, 177(3), 1091-1110.  
 Lin, F. C., & Ritzwoller, M. H. (2011). Helmholtz surface wave tomography for isotropic and azimuthally anisotropic structure. *Geophysical Journal International*, 186(3), 1104-1120.  
 Lu, Y. (2019). Tomography of the alpine arc using noise correlations & waveform modelling (Doctoral dissertation).  
 Pieri, M., and Groppi, G. (1981). Subsurface geological structure of the Po plain, Italy. *Cons. Naz. Delle Ric. Agip*, Rome 414.  
 Kästle, E. D., El-Sharkawy, A., Boschi, L., Meier, T., Rosenberg, C., Bellalun, N., ... & Weidler, C. (2018). Surface wave tomography of the alps using ambient-noise and earthquake phase velocity measurements. *Journal of Geophysical Research: Solid Earth*, 123(2), 1770-1792.  
 Kern, H. (1990). Laboratory seismic measurements: an aid in the interpretation of seismic field data. *Terra Nova*, 2(6), 617-628.  
 Nicolas, A., & Christensen, N. I. (1987). Formation of anisotropy in upper mantle peridotites-A review. *Composition, structure and dynamics of the lithosphere-asthenosphere system*, 16, 111-123.